

Electronic Supplementary Information
**Isotachophoresis with ionic spacer and two-stage separation
for high sensitivity DNA hybridization assay**

Charbel Eid^a, Giancarlo Garcia-Schwarz^a, and Juan G. Santiago^{a,*}

^a*Department of Mechanical Engineering, Stanford University, CA 94305, USA.*

Contents

Section S1: Materials and Reagents

Section S2: Experimental setup and apparatus

Section S3: Chip layout and assay protocol

Section S4: Effect of sieving matrix on small ion mobility

Section S5: Gaussian filtering using a seven point kernel

Section S6: Data analysis technique

Figure S1: Layout of microfluidic chip used for all experiments

Figure S2: Comparison of measured voltage in the presence and absence of polymer sieving matrix

Figure S3: Gaussian filtering of raw experimental data

Figure S4: Demonstration of data analysis method

Figure S5: Fluorescent signal for limit of detection study

Table S1: Probe and target oligonucleotide sequence and predicted melting temperature

Table S2: Electrode location at the different stages of the assay

Section S1. Materials and reagents

We purchased 3-(N-morpholino)propanesulfonic acid (MOPS), 4-(2-Hydroxyethyl)piperazine-1-ethanesulfonic (HEPES), trizma base, and hydroxyethyl cellulose (HEC, MW = 250,000) from Sigma-Aldrich (St. Louis, MO). Pre-pared UltraPure 1M Tris-HCl (pH 8.0) and DNase/RNase-free distilled water were obtained from Invitrogen (Life Technologies, Carlsbad, CA). We purchased hydrochloric acid from J.T. Baker (Avantor Performance Materials, Center Valley, PA). Sodium hydroxide was procured from Mallinckrodt Chemicals (Avantor Performance Materials, Center Valley, PA). We purchased Urea and magnesium chloride from EMD Millipore (Gibbstown, NJ). Polyvinylpyrrolidone (PVP, MW = 1,000,000) was obtained from Polysciences, Inc. (Warrington, PA).

We obtained the polyacrylamide gel (PAGE)-purified synthetic DNA oligonucleotides from Genelink (Hawthorne, NY). The sequences are shown in **Table S1**. We reconstituted the oligonucleotides in 10 mM Tris-HCl buffer. Further dilutions were prepared in 20 mM Tris-HEPES buffer. Stock solutions were stored in -20°C. DNA solutions were kept in 4°C for short-term usage. We purchased Crown glass microfluidic chips (model NS260) from Caliper Life Sciences (Mountain View, CA). Chip geometry and layout is detailed in **Figure S1**.

Section S2. Experimental setup and apparatus

Experimental visualizations were performed on an epifluorescent microscopy setup. The components of the setup include an inverted epifluorescent microscope (Eclipse TE200, Nikon, Melville, NY) equipped with 4x and 10x objectives (PlanApo, Nikon, Melville, NY) and Cy5 filter cube (XF110-2, Omega, Brattleboro, VT). Illumination was provided by a 100 W short-arc mercury lamp (102DH, Ushio, Tokyo, Japan). The microscope was connected to a coupled charge device (CCD) camera (Coolsnap, Roper Scientific, Trenton, NJ). We triggered the microscope with a function generator (Model 555, Berkeley Nucleonics, San Rafael, CA). We used a high-voltage sourcemeter (2410, Keithley Instruments, Cleveland, OH) and applied constant current (at 2.5 μ A) to the chip. We controlled the sourcemeter and recorded data using a custom MATLAB (R2011a, Mathworks, Natick, MA) script.

Data acquisition was performed using a custom built point-confocal epifluorescent microscopy setup, described by Bercovici et al.¹ and Garcia-Schwarz and Santiago.² We refer to Garcia-Schwarz and Santiago. for a detailed schematic of the experimental setup (see their Supplemental Information document). Briefly, the setup consists of an inverted epifluorescent microscope (IX70, Olympus, Hauppauge, NY) equipped with 60x water-immersion objective (LUMPlanFL, Olympus, Hauppauge, NY) and Cy5 filter cube (Cy5-4040A, Semrock, Rochester, NY). An automated stage (ASI, Eugene, OR) was used to adjust chip location and focus. Illumination was provided by a 642 nm diode laser (Stradus-642, Vortran Laser Technologies, Sacramento, CA). The microscope was also connected to a photomultiplier tube (PMT) model (H6780-20, Hamamatsu Photonics, Hamamatsu, Japan) with data acquisition unit (C8908, Hamamatsu Photonics, Hamamatsu, Japan) for detection. The PMT was triggered by a function generator (E3631A, Agilent Technologies, Santa Clara, CA) and operated at a rate of 66.7 Hz (with 10 ms integration time). We used a high-voltage sourcemeter (2410, Keithley Instruments, Cleveland, OH) and applied constant current (at 2.5 μ A) to the chip. We controlled both the PMT and sourcemeter and recorded data using a custom MATLAB (R2007b, Mathworks, Natick, MA) script.

Table S1. Sequence of the synthetic DNA oligonucleotides used here as well as melting temperatures (T_m) as predicted by the manufacturer.. Both oligonucleotides are purified by polyacrylamide gel electrophoresis (PAGE).

Description	Sequence	T_m (°C)
27 nt probe	5-/Cy5/ CAT CGT TTA CGG CGT GGA CTA CCA GGG -3	66.9
149 nt target	5- ATT GGG AGT GGT TGA TGC TCT ATA CTC CAG TAG CAA GGC ACT TCC GGA CTC AAT GAA GGG CCG GGA CCC TGG TAG TCC ACG CCG TAA ACG ATG AAG GAG CCA ATA CAA AGG CTT CAT CCT CAC TCG CAT GGA GGC AAA CGC AGA ACA AT- 3	80.6

Section S3. Chip layout and assay protocol

Before each run, we rinsed the chip to clean and prepare the glass channel surfaces for experiments. By rinsing, we refer to the process of injecting a volume into the reservoirs, followed by applying vacuum at reservoir 6 to fill the rest of the channel. The process was carried out in the following steps:

1. Rinse with deionized (DI) water for 10 min
2. Rinse with 1M sodium hydroxide for 5 min
3. Rinse with 1M hydrochloric acid for 5 min
4. Rinse with DI water for 10 min

Immediately following this process, we loaded the chip and ran the assay as follows:

1. Pipette 10 μ L of LE1 into reservoirs 1, 2, 3, 4, 5, 6 and 10 μ L of LE2 into reservoirs 7 and 8.
2. Apply vacuum at reservoir 6 to fill the channel with the buffer solutions LE1 and LE2.
3. Quickly empty reservoirs 1 and 4, clean with a small amount of DI water, and pipette TE into reservoir 4 and TE+sample into reservoir 1.
4. Place the ground electrode in reservoir 1 and the high with reservoir 8. As soon as the sample zone reaches the pre-determined observation point, switch the ground electrode from reservoir 1 to reservoir 4. This process is described in **Table S2** below.

During the injection phase, we applied 1 mW of laser power. In the detection phase, however, the laser powered applied depended on the target concentration. For the negative control as well as at target concentrations of 220 fM and 760 fM, we used 110 mW of laser power. We used 1 mW for higher concentrations, including 76 pM, 760 pM, 7.6 nM, and 76 nM. At 7.6 pM, we used both 1 and 110 mW in order to compute a conversion factor between 1 and 110 mW laser powers. This conversion factor was necessary due to slight photobleaching that may occur at higher laser powers and any differences in quantum yield (e.g., due to saturation of the fluorescence rate). We found this conversion factor to be 37.75 (i.e., 1 fluorescence unit at 1 mW is equivalent to 37.75 units at 110 mW.)

Table S2. Electrode arrangement for injection and detection steps. Termination of the injection and detection phases was triggered by the arrival of the sample plug into a fixed observation point. We applied 2.5 μ A constant current between ground (GND) and positive (HI).

Step	Approximate Duration (s)	Reservoir							
		1	2	3	4	5	6	7	8
Injection	190	GND	-	-	-	-	-	-	HI
Detection	380	-	-	-	GND	-	-	-	HI

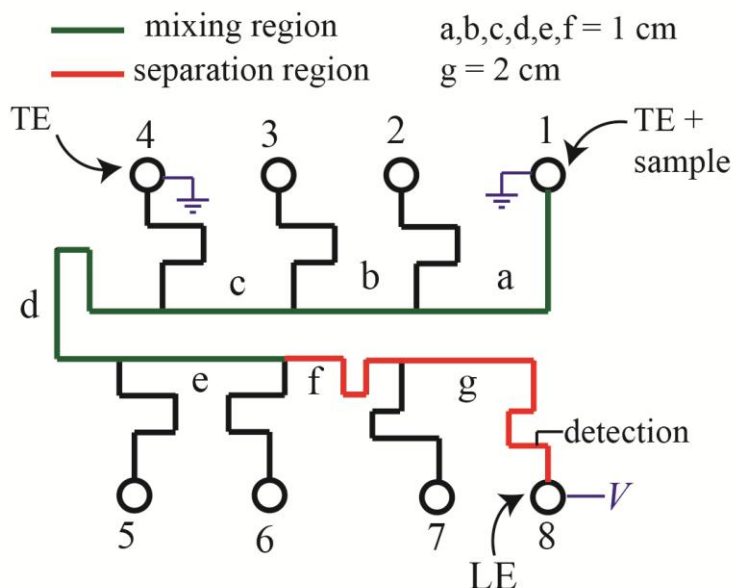


Figure S1. Layout of microfluidic Crown glass chip used for all experiments. The mixing region (green) contains LE with no sieving matrix present. The separation region (red) contains LE along with 1.8% HEC polymer. TE, TE + sample, and LE were all dispensed into their respective reservoirs prior to the application of electric field. The procedure for loading chip and applying voltage is described in Section S3 and Table S1. The first observation point was located a few millimeters beyond reservoir 4. When the sample plug reached that point, we observed a peak in the signal, attributed to the fluorescence of the probe molecules. At this point, the GND was switched from reservoir 1 to reservoir 4 for the remainder of the experiment.

Section S4. Effect of sieving matrix on small ion mobility

In obtaining an estimate for the mobility of the probe-target complex based on eq. 1, we stated the assumption that the mobility of small ions is unaffected by the presence of a sieving matrix. We use this assumption to obtain the electric field as computed in the SPRESSO software package. We set out to examine the impact of including a sieving matrix in the buffer on the mobility of the ions. We chose to infer the mobility indirectly by measuring the voltage using the same set-up described in the other sections. The relation between voltage and mobility can be shown briefly. Ohm's Law, as well as the definitions of electrical resistance and conductivity yield the following equations:

$$V = RI \quad (\text{eq. S1})$$

$$R = \frac{l}{\sigma A} \quad (\text{eq. S2})$$

$$\sigma = \sum_i \sum_{z=n_i}^{p_i} z_i F c_{i,z} \mu_{i,z} \quad (\text{eq. S3})$$

We chose to perform this evaluation of small ion mobility using potassium chloride (KCl). The two ions comprising the electrolyte, K^+ and Cl^- , are monovalent and have similar mobilities,³ therefore making them suitable for this analysis. After some algebraic manipulation, eq. S1 can be rewritten as:

$$V = \frac{LI}{FA} \frac{1}{(c_{K^+} \mu_{K^+} + c_{Cl^-} \mu_{Cl^-})} \quad (\text{eq. S4})$$

In a solution of 100 mM KCl, the concentration of the ions is equal ($c_{K^+} = c_{Cl^-} = c$). The mobilities of K^+ and Cl^- are assumed approximately equal ($\mu_{K^+} = \mu_{Cl^-} = \mu$), which leads to the simplified version of eq. S4:

$$V = \frac{LI}{FA} \frac{1}{c\mu}$$

Therefore, by using the same chip (L and A are constant), supplying the same amount of current (I is constant), and using the same concentration solution (c is constant), the change in voltage will be inversely proportional to the increase in mobility. We thus ran two sets of experiments, supplying $5.5 \mu A$ of current and using a 100 mM KCl solution. The first set included no HEC polymer, while the second one included 1.5% HEC. Results of these experiments are shown in **Fig. S2**, and indicate that HEC does not significantly affect mobility of these small ions.

To corroborate this result, we also measured the conductivity of KCl solutions with and without HEC directly using a conductivity meter (not shown). These experiments confirmed our initial findings. The results in **Fig. S2** even indicate a minor increase in the conductivity, but we know of no physical basis to indicate that the mobility of ions increases in the presence of sieving matrix. We therefore attribute this difference to incomplete surface equilibration and/or small temperature differences between experiments. In our ITP assay analysis, we made the assumption that the mobility of the LE ions was the same in free solution as is in the presence of a sieving matrix.

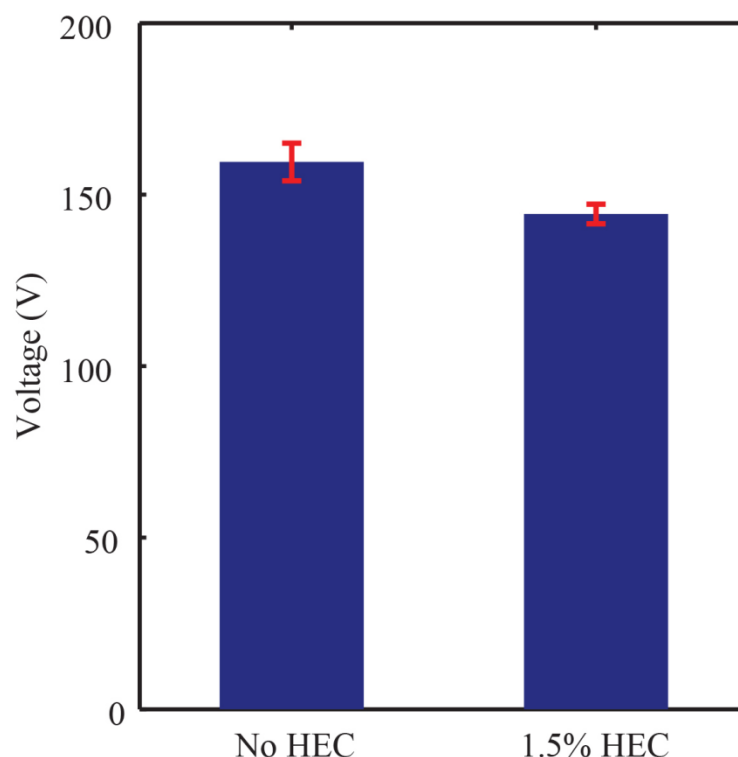


Figure S2. Measurements quantifying the impact of sieving matrix on the mobility of an electrolyte buffer. Measured voltage is inversely proportional to mobility, and thus provides a method to infer information about mobility. We performed two sets of experiments involving 100 mM KCl buffer in a microfluidic channel. In the first set the buffer contained no HEC polymer, while in the second we included 1.5% HEC in the buffer. We applied $5.5 \mu A$ of constant current in all experiments and

measured mean voltages of 159.5 V and 144.3 V, respectively. A decrease in mobility corresponds to an increase in measured voltage. We see no indication of that, and instead observe a slight decrease in the voltage. We therefore assume that the sieving matrix does not significantly affect the mobility of these small ions.

Section S5. Gaussian filtering using a seven point kernel

In order to eliminate high-frequency noise in the raw experimental data, we performed Gaussian filtering on all obtained data. Gaussian filtering convolves a Gaussian function with the raw data. The Gaussian function is characterized by a standard deviation width equal to double the 15 ms sampling period of the PMT), and is normalized in order to keep the sum of the values in the filter at unity. We used a seven point Gaussian kernel, and performed all processing using MATLAB. **Fig. S3** shows the pre- and post-filtering data for a limit of detection (220 fM) experiment.

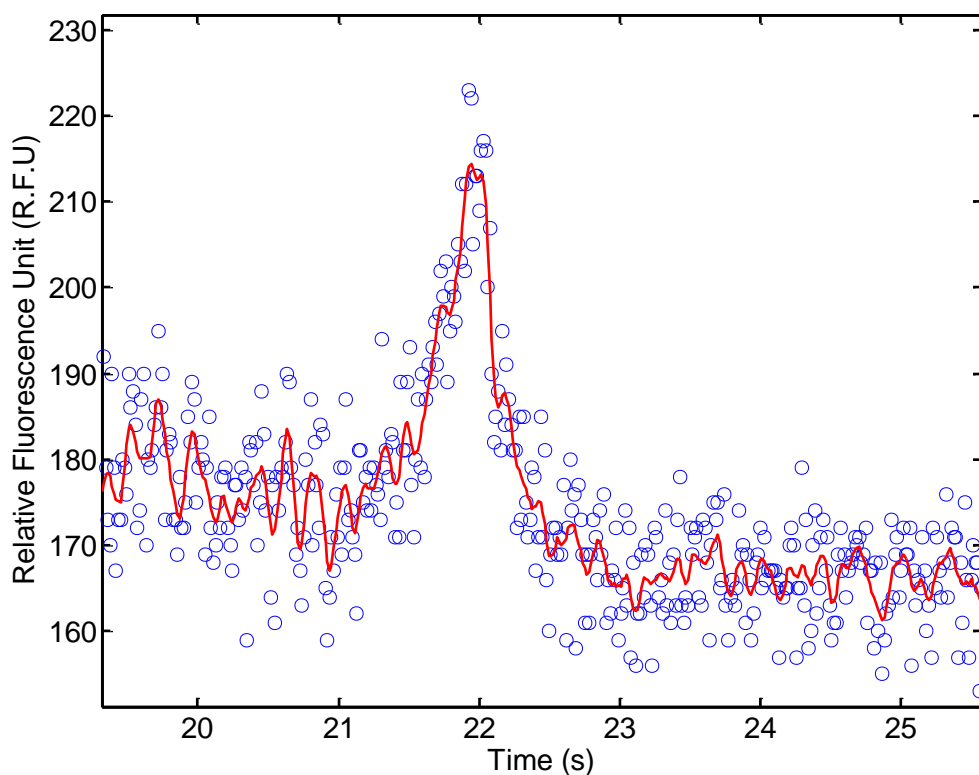


Figure S3. Raw fluorescence data (circles) plotted along with the Gaussian filtered signal (solid line) from an arbitrary run using 220 fM target. Gaussian filtering using a normalized Gaussian curve with width equaling twice the sampling period of the PMT. Note the difference in background noise levels preceding (19.5 – 21 s) and following (23 – 25.5 s) the peak. These data as shown here are not background adjusted.

Section S6. Data analysis technique

In all experiments, we observed incongruence in the noise floor before and after the trailing peak. An example of this can be observed in **Fig. S3**, as the noise floor up to 21 s and that after 23 s converge at different baseline values. The trailing peak is preceded by a leading peak, which is comprised of unreacted probe molecules. We hypothesized that the high noise level between the two peaks is due to probe impurity, as well as trace amounts of dimerized target or probe molecules. Optimizing the

concentration of the sieving matrix aided in minimizing this noise, but we were unable to completely remove it. This issue was only relevant at the lowest concentrations, where the signal-to-noise ratio is relatively low. We thus chose to account for the discontinuous noise floor levels by modifying our peak integration method. We wrote a script that locates the maximum value of the Gaussian filtered signal, and forms a fit of the five points on each side of the maximum. This results in an 11-point fit used for computing the integral. In this way, the fit includes information about the amplitude of the peak and its width but more strongly emphasizes the highest magnitude regions of the peak. **Fig. S4** demonstrates this method, using an arbitrary run with 7.6 pM of target. In **Fig. S5**, we overlay three representative runs of the negative control as well as the lowest two target concentrations, and demonstrate the combined Gaussian filtering and the chosen data analysis technique.

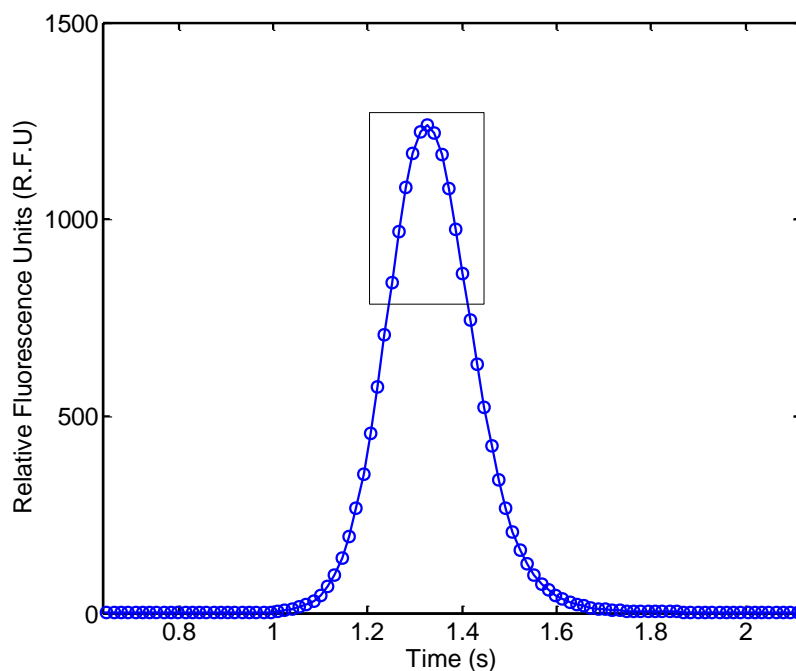


Figure S4. Demonstration of the data analysis used to integrate over the trailing peak in the signal data. The rectangular box indicates the 11 points that comprise the fit, consisting of point of maximum signal along with the adjacent 5 points preceding and following it. We then sum over the 11 points to compute the signal associated with the peak. We do this for both the leading and trailing peaks in all the runs. The above plot is taken from an arbitrarily-chosen, background-adjusted experiment containing 7.6 pM target.

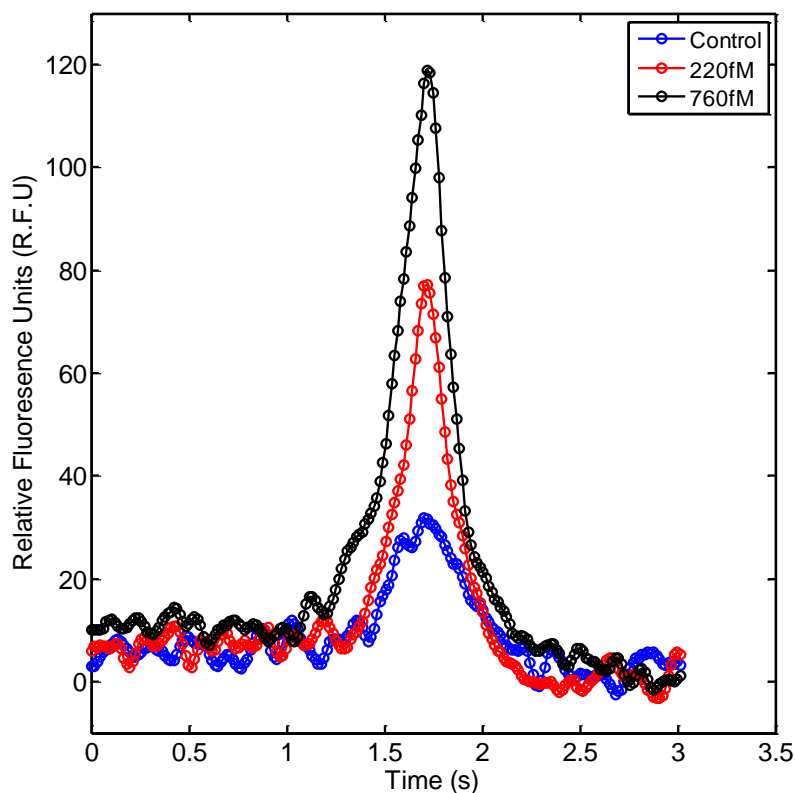


Figure S5. Plots of the Gaussian filtered data (as described in **Section S5**) for the trailing peak in the negative control as well as lowest target concentration cases (with 220 and 760 fM target). The peak signals are stacked on top of each other for easy comparison. The origin on the abscissa is set to the point at which the laser power is switched to 110 mW.

References:

- 1 M. Bercovici, G.V. Kaigala, K. E. Mach, C. M. Han, J. C. Liao, J. G. Santiago, *Anal. Chem.* **2011**, *83*, 4110-4117.
- 2 G. Garcia-Schwarz, J. G. Santiago, *Anal. Chem.*, 2012, **84**, 6366-6369.
- 3 H. E. Gunning, A. R. Gordon, *J. Chem. Phys.*, 1942, **10**, 126-131.